Electronic Supplementary Information (ESI)

Controllable Silicon Nanostructures Featuring Stable Fluorescence and Intrinsic *In Vitro* and *In Vivo* Anti-Cancer Activity

Binbin Chu, ‡ Sicong Wu, ‡ Xiaoyuan Ji, Runzhi Chen, Bin Song, Jiali Tang, Houyu Wang, Yuanyuan Su and Yao He*

Laboratory of Nanoscale Biochemical Analysis, Institute of Functional Nano & Soft Materials (FUNSOM), and Collaborative Innovation Center of Suzhou Nano Science and Technology (NANO-CIC), Soochow University, Suzhou, Jiangsu 215123, China.

E-mail: yaohe@suda.edu.cn (Yao He)

List of Contents

1. Experimental section

1.1 Reagents and apparatus

All chemicals were analytical grade and used without additional purification. The (3-aminopropyl) trimethoxysiliane (97%) was purchased from Sigma-Aldrich (Shanghai, China). [1-5] Phosphate buffered saline (PBS) solutions were obtained from Cindiff Bioscientific Co., Ltd. (Shanghai, China). All of four green teas (including Anji white tea (WT), longjing (LJ), gougunao (GGN), and biluochun (BLC)) were supplied by the Auchan (China) investment Co., Ltd. or Tmall (China) online mall (https://www.tmall.com/). In particular, gougunao tea with the trade marker of Jing-Gang-Si-Yuan were grown in Ji'an City of Shanxi Province, longjing tea with the trade marker of Xi-Hu-Long-Jing were grown in Hangzhou City of Zhejiang Province, biluochun tea with the trade marker of Yi-Nong were grown in Suzhou City of Jiangsu Province, and Anji white tea with the trade marker of An-Ji-Bai-Cha were grown in An'ji County of Zhejiang Province. Note that four kinds of green tea were only bought from above companies without any special mentions in following experiments. Dulbecco's modified eagle media (DMEM), RPMI-1640 media, F-12 media, fetal bovine serum, penicillin (100 μg/mL), and streptomycin (100 μg/mL) were obtained from Invitrogen corporation (Life Technologies, Shanghai, China). PicoGreen® dsDNA assay kit was obtained from Thermo Fisher Scientific (Shanghai, China). Propidium iodide (PI) was purchased form Beyotime Biotechnology (Shanghai, China). All solutions were prepared using distilled water (Millipore).

The GTSN were synthesized via the microwave system NOVA (Preekem, China), operating at 2450 MHz, 0-500 W. The GTSN were characterized by transmission electronic microscopy (TEM) and high-resolution TEM (HRTEM), using an electron microscope (Philips CM 200) with 200 kV. [1-5] A 750 UV-vis near-infrared spectrophotometer (Perkin-Elmer lambda) was used for measurement of UV-vis absorption spectra. A spectro-fluorimeter (HORIBA JOBIN YVON FLUORMAX-4) was employed for recording photoluminescence (PL). A Fourier-transform infrared (FTIR) spectrometer (Bruker HYPERION) was used for the characterization of FTIR spectra. Delsa™ nano submicron particle size (Beckman Coulter, Inc) was employed for the analysis of dynamic light scattering (DLS). The microplate photometer (Bio-Rad 680, U.S.A.) was used to determine the absorbance OD value of resultant cells with different treatment. FACS Calibur flow cytometry (FACS Calibur from Becton, Dickinson and Company) was employed for analysis of cell cycle of different selected cell lines. Fluorescence imaging experiments were performed on a confocal laser scanning microscope (CLSM, Leica, TCS-SP5 II). In vivo fluorescence image of these mice with different treatment is captured by a Maestro EX in vivo fluorescence imaging system (CRi, Inc.).

1.2 The TEM and HRTEM images of the GTSN

Samples for TEM analysis were prepared by placing 10 μL of the four kinds of GTSN, *i.e.,* WT-SiNPs, LJ-SiNPs, GGN-SiNShs or BLC-SiNSps solution, on the carbon-coated copper grid and then drying at room temperature. The morphologies of the four types of resultant GTSN (*e.g.,* WT-SiNPs, LJ-SiNPs, GGN-SiNShs, or BLC-SiNSps) were characterized by TEM and high-resolution TEM (HRTEM).

1.3 Cellular morphology analysis

Firstly, cancer these cells (including HeLa, MCF-7, B16, and PC-3 cells) were dispersed in 96-well cell-culture plate at a density of 1.5×10^4 cells/well, and incubated with the fluorescent GTSN and pure green tea solutions with the same concentration of 10.00 mg/mL at 37 ^oC for 24 h. Meanwhile, normal cells (including ARPE-19 and HFF-1 cells) were dispersed in 96-well cell-culture plate at a density of 2.0×10^4 cells/well, and incubated with the fluorescent GTSN and pure green tea solutions at same concentration of 2.50 mg/mL at 37 ^oC for 24 h. Then, these cellular morphologies of various cell lines were captured by using a common fluorescence microscope.

1.4 Cell cytoskeleton formation

HeLa, MCF-7, B16, and PC-3 cells are cultured on 24-well plates with cover slips at 1.5×10^5/well at 37 ^oC under 5% CO2 for overnight. And then, these prepared cells (e.g., HeLa, MCF-7, B16, and PC-3 cells) were incubated with determined concentrations of GTSN (e.g., 10.00 mg/mL) for another 24 h, respectively. After treatment, cells are fixed with 4% paraformaldehyde-4% sucrose for 25 min and blocked with PBS containing 4% BSA and 0.1% Trinton X-100 for 1 h. The cytoskeleton is labeled with 300 nM rhodamine-labeled phalloidin (Sigma, Shanghai) for 2 h, followed by washing with PBS containing 0.1% Tween 20 for three times. The resultant cells are finally observed by CLSM (Leica, Germany).

1.5 Photostability comparison of fluorescent GTSN

Firstly, antibiotics (100 μg/mL streptomycin and 100 U/mL penicillin) and RPMI-1640 with 10% heat-inactivated fetal bovine serum (FBS), served as cellular culture medium, were first used for culturing breast cancer cells (MCF-7 cells) in the humidified atmosphere with 5% CO_2 at 37 ^oC overnight. After that, 4% sucrose and 4% paraformaldehyde were employed for fixing the MCF-7 cells for 25 min, followed by 60-min blocking in PBS containing 4% BSA and 0.1% Triton X-100. PBS containing 0.1% Tween 20 was then utilized to wash the fixed MCF-7 cells over three times. For labeling microfilaments, the resultant cells were first incubated with rhodamine-phalloidine for 2 h. Afterwards, for labeling nuclei, the treated cells were incubated with the fluorescent GTSN (10.00 mg/mL) for 2 h. Finally, the resultant samples were mounted on slides in fluoromount (Sigma, F4680), and captured by a confocal laser microscope. For labeling nuclei, diode laser ($\lambda_{excitation}$ = 405 nm) was used as the excitation light source. For labeling microfilaments, diode laser ($\lambda_{excitation}$ = 543 nm) was used as the excitation light source. Detection windows for fluorescent GTSN and rhodamine-phalloidine are 425-520 and 560-620 nm, respectively. For control experiments, the power of diode laser ($\lambda_{excitation}$ = 405 nm or 543 nm) was the same. A cooled CCD camera was used for capturing the confocal images at 30 sec intervals, which were then analyzed through image analysis software (LAS AF Lite).

1.6 Long-term and real-time intracellular tracking of the resultant GTSN

To verify the feasibility of the resultant GTSN for long-term and real-time cellular tracking in living HeLa cells, a time relapse experiment at a time interval of 30 sec was designed to visualize the cellular uptake process when HeLa cells were treated with as-prepared fluorescent GTSN (10.00 mg/mL) and the total time lasted for 60 min. In detail, the HeLa cells were incubated with

H-DMEM medium for 24 h at 37 °C followed by washing with PBS buffer. Afterwards, the as-prepared fluorescent GTSN-treated cell lines (HeLa cells) immediately suffer continuous UV irradiation up to 60 min under the microscopy. The images of fluorescent GTSN channels were collected at 425-520 nm with excitation at 405 nm through a 63 × 1.4 NA objective.

1.7 Cell apoptosis/death and cell cycle phase analysis

Propidium iodide (PI) single staining method was performed to analyze cell apoptosis and death which were treated by pure green tea solutions or the resultant GTSN. In detail, cancer cells (e.g., HeLa, MCF-7, B16, and PC-3 cells) and normal cells (e.g., ARPE-19 and HFF-1 cells) were firstly seeded into 6-well plates (2.5×10^5/well) at 37 ^oC under 5% CO_2 for 24 h. And then, these resultant cells were incubated with four kinds of pure green tea solution or GTSN at the same concentration of 2.50 mg/mL for another 24 h, respectively. After that, these prepared adherent cells were detached by the addition of trypsin, washed with PBS and collected by refrigerated centrifugation. Then resultant cells were resuspended in ice-cold PBS, and then fixed with 70% precooled ethanol at -20 ^oC for over 2 h. Ethanol-fixed cells were washed twice with ice-cold PBS containing with 2% BSA again, and then incubated with 1 mg/mL RNase A for 20 min at 37 ^oC, and stained with 10 mg/mL PI for 30 min in the dark. The cell apoptosis and death finally were measured on a FACS Calibur flow cytometry (FACS Calibur from Becton, Dickinson and Company).

For analyzing cell cycle phase of the GTSN-treated cells, the PI single staining method combined with flow cytometry was also performed in the following experiments. In brief, cancer cells (e.g., HeLa, MCF-7, B16, and PC-3 cells) were firstly seeded with 2.5×10^5/well in 6-well plates. After incubated for 24 h, pure medium, pure green tea solutions (2.50 mg/mL), and the four kinds of GTSN (2.50 mg/mL) dissolved in culture medium were added to each well. After another 12-h incubation, these prepared cells were harvested, fixed in 70% ethanol and stored at -20 ^oC. Cells were then washed twice with ice cold PBS and incubated with RNase and DNA intercalating dye PI for 30 min in dark, and cell cycle phase analysis was performed using a BD FACS Calibur flow cytometer (FACS Calibur from Becton, Dickinson and Company).

For analyzing cell apoptosis/death and cell cycle phase, the FlowJo software was used to analyze the data obtained from above BD FACS Calibur flow cytometer.

1.8 Hemolysis assay

Healthy mice blood (8 mL) was achieved from experimental female mice. RBCs were collected by centrifugation at 3000 rpm for 10 min, washed with normal saline (0.9% NaCl) for three times, and resuspended using normal saline (100 mL) to prepare 2% erythrocyte solution. Then, different concentrations (0, 0.63, 1.25, 2.50, 5.00, and 10.00 mg/mL) of fluorescent GTSN dissolved in normal saline solutions were added to the same-volume 2% erythrocyte solution in centrifuge tubes. After incubation at 37 ^oC for 5 h, the supernatant was obtained through centrifugation at 3000 rpm for 10 min, and transferred to a 96-well plate. The absorbance at 450 nm was measured by a microplate photometer (Bio-Rad 680, U.S.A.). RBCs in normal saline and in 1% Triton X-100 in normal saline were used as a negative control and a positive control, respectively. The following formula was used to calculate the hemolysis percentage:

Hemolysis (%) = (mean of absorbance value of treated group - mean of absorbance value of negative control group) / (mean of absorbance value of positive control - mean of absorbance value of negative control group) × 100%.

1.9 Histology analysis and Blood analysis

14 days after physiological saline (untreated), pure green tea solutions (i.e., WT, LJ, GGN, and BLC solutions), and four kinds of GTSN (i.e., WT-SiNPs, LJ-SiNPs, GGN-SiNShs, and BLC-SiNSps) injection, the treated mice were sacrificed for harvesting major organs (e.g., heart, liver, spleen, lungs, kidneys and brain), which were fixed and processed in formalin (10%) and paraffin, respectively. Afterwards, the organ tissues were sectioned as 10 microns, followed by staining with hematoxylin & eosin (H & E), and finally examination using a digital microscope. Blood was harvested from the orbital sinus via rapid removal of the eyeball from mice intratumorally injected with physiological saline, pure green tea solutions (i.e., WT, LJ, GGN, and BLC solutions), and four kinds of GTSN (i.e., WT-SiNPs, LJ-SiNPs, GGN-SiNShs, and BLC-SiNSps) at the same dose of 50 mg/kg after 0, 7, and 14 days (three mice per group). The resultant blood samples were used for serum biochemistry and complete blood count assays.

2. TEM images of pure green tea after microwave irradiation

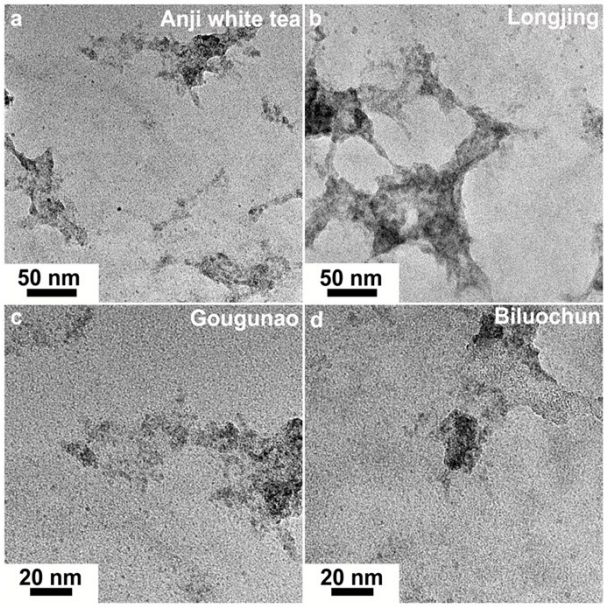

Figure S1. TEM images of pure green tea after microwave irradiation. TEM images of pure Anji white tea (a), longjing (b), gougunao (c), and biluochun (d) after microwave irradiation.

As shown in Figure S1, the TEM images of pure Anji white tea, longjing, gougunao, and biluochun compound exhibit no obvious nanostructures and ambiguous morphologies.

3. AFM images and reaction mechanism of 0D WT-SiNPs and LJ-SiNPs

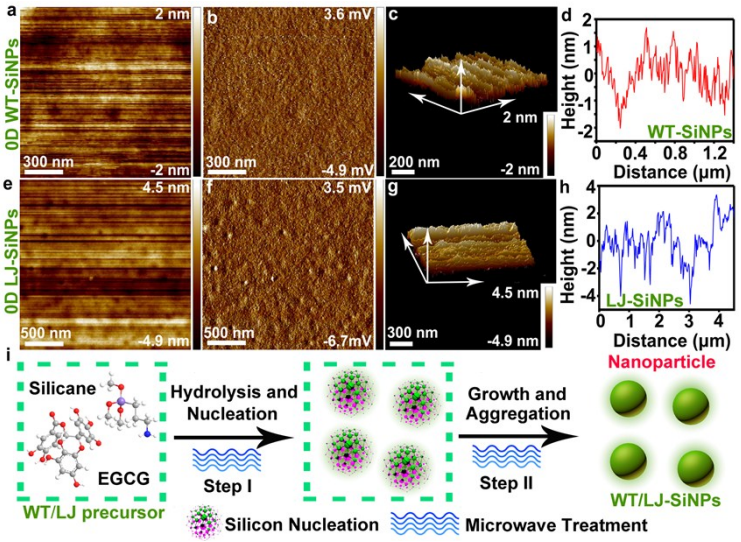

Figure S2. AFM images and possible reaction mechanism of 0D WT-SiNPs and LJ-SiNPs. (a-c) AFM images and 3D images of GGN-SiNShs. (d) Scatter diagrams of height of AFM images originated from the Figure S2c. (e-g) AFM images and 3D images of GGN-SiNShs. (h) Scatter diagrams of height of AFM images originated from the Figure S2g. (i) Proposed synthesis mechanism of the fluorescent WT-SiNPs or LJ-SiNPs under microwave-assisted treatment.

As displayed in AFM images (Figures S2a-d), the samples of WT-SiNPs on substrates are much smooth with a surface roughness of ~2.0-4.0 nm, showing the existence of very small particles building the sample's films. Meanwhile, the samples of LJ-SiNPs on substrates show similar surface roughness of ~4.5 nm (Figures S2e-h), revealing the dot-like nanostructures of LJ-SiNPs. Based on the experimental results, a possible reaction mechanism is proposed as follow. We hypothesize that both WT and LJ tea mostly containing (-)-epigallocatechin-3-gallate (EGCG) may act as a reductant for reducing $C_6H_{17}NO_3Si$ molecules under microwave irradiation, leading to the creation of Si nanoclusters (step I, Figure S2i); [1, 3-6] afterwards, the nanoclusters, served as nuclei, are further growth *via* Ostwald Ripening mechanism to produce dot-like nanostructures (step II, Figure S2i). [1, 3-6]

4. AFM images and possible reaction mechanism of 2D GGN-SiNShs

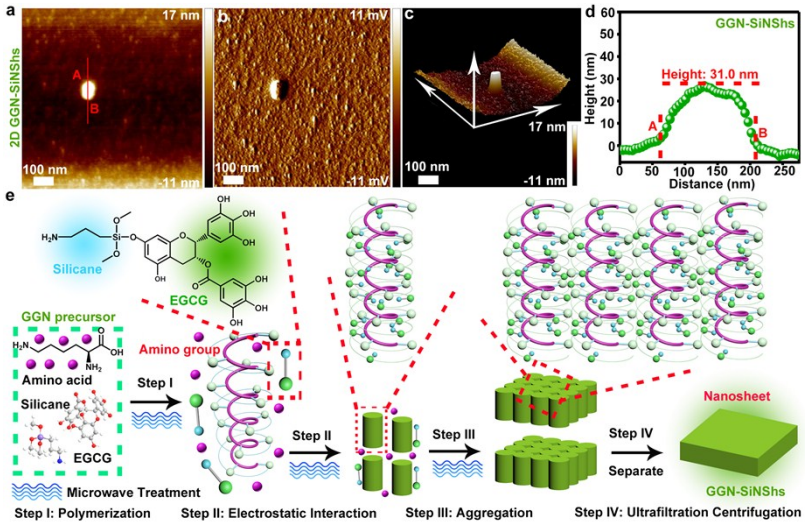

Figure S3. AFM images and possible reaction mechanism of 2D GGN-SiNShs. (a-c) AFM images and 3D images of GGN-SiNShs. (d) Scatter diagrams of height of AFM images originated from Figure S3c. (e) Proposed synthesis mechanism of the fluorescent GGN-SiNShs under microwave-assisted treatment.

The AFM images provide further evidence for confirming 2D square structures of the GGN-SiNShs (Figure S3a-d). In detail, these edges of GGN-SiNShs (Figure S3a) could be clearly observed even for the underlying nanostructured sheets (Figure S3b), indicating their 2D character (Figure S3c). By line scanning across the plain area of the sheet, the height is estimated to be approximately 31.0 nm (Figure S3d), thus providing evidence that the substance in the colloidal solution indeed consisted of nanosheets structures. Based on above experimental results, a possible reaction mechanism is proposed as follow. Lysine, known as one kind of the amino acid (Tables S1-2) mainly existed in the GGN, may play a critical role for synthesizing GGN-SiNShs with square nanostructures, which has been previously used to control Si-based nanomaterials with various nanostructures (*e.g.,* hexagons, square, *etc.*). [7-11] Typically, the lysine in precursor can form poly(L-lysine) (PLL) through polymerization, and then other phosphate ions (Table S1) in GGN solutions and silicane could induce a random coil to α-helix transition in the secondary structure of PLL (Figure S3e, Step I). [7] Meanwhile, the EGCG and silicane molecules can also produce the EGCG-silicane composites (EGCG-Si) (Figure S3e, Step I). [3-6] After that, the hydrophobic groups of EGCG-Si bind preferentially to the grooves between the amino groups of PLL, whereas anionic hydroxy group of EGCG-Si emerge on the surface, forming distinct helical strands (Figure S3e, Step II). [10] Neighboring PLL helices are further thought to be bound together through multiple interactions, leading to the production of the GGN-SiNShs with square-like nanostructures (Figure S3e, Step III-IV). [7-11]

5. AFM images and possible reaction mechanism of 3D BLC-SiNSps

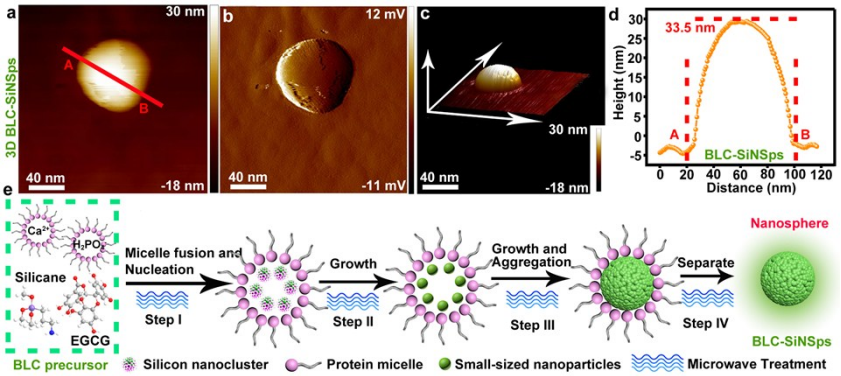

Figure S4. AFM images and possible reaction mechanism of 3D BLC-SiNSps. (a-c) AFM images and 3D images of 3D BLC-SiNSps. (d) Scatter diagrams of height of AFM images originated from Figure S4c. (e) Proposed synthesis mechanism of fluorescent 3D BLC-SiNSps under microwave-assisted treatment.

AFM images display distinct edges of the spheroidal nanostructure with estimated height of ~33.5 nm, providing the further evidence of the 3D nanostructures of BLC-SiNSps (Figure S4a-d). Based on above experimental results and discussions, a possible reaction mechanism is proposed as follow. In this case, the silicane molecules (*e.g.,* $C_6H_{17}NO_3Si$, *etc.*) could interact with EGCG contained in precursor; and meanwhile the albumens (one of the proteins existed in BLC tea, Tables S1-2) could be pyrolyzed through microwave irradiation, leading to the creation of Si nanoclusters (Figure S4e, Step I). [12-15] Then, these incompact Si nanoclusters can assemble and further grow into small-sized nanoparticles (*e.g.,* tea saponin, carbohydrate, *etc.* Table S1) in BLC solutions (Figure S4e, Step II) under microwave irradiation. [15] After that, these small-sized nanoparticles would continue to grow and aggregate into larger nanospheres under interactions of surfactant molecules (Figure S4e, Step III). [12-15] Finally, the BLC-SiNSps could be obtained after purification (Figure S4e, Step IV).

6. Comparison of the major chemical components of green tea

Table S1. Contents of major chemical components in green tea. [16-21]

Composition [a]	Content (%)	Chemical components [b]
Tea polyphenols (TP)	~24-36	*e.g.,* EGCG, catechin, theaflavin, *etc.*
Protein	~20-30	*e.g.,* albumin, glutelin, globulin, *etc.*
Amino acids (AA) [c]	~1-4	*e.g.,* theanine, lysine, *etc.* [22-24]
Minerals [25]	~3.5-7.0	*e.g.,* K, P, Ca, Mg, Fe, Mn, *etc.*
Carbohydrate	~20-25	*e.g.,* tea polysaccharide, cellulose, *etc.*
Lipoid [d]	~8	*e.g.,* tea saponin, phospholipid, *etc.*
Others [e]	~0.03-5	*e.g.,* vitamin, pigment, aromatic, *etc.*

[a] The main composition of green tea is easily obtained from the Internet. [b] Each composition contains many similar chemical components. [c] Amino acids content is quality indicators for leaf teas and teabags. [23, 24] [d] Tea saponin, known as one of the glycoside compounds, can be used as important surfactants in our systems. [e] Vitamin contains vitamin C, A, D, E, B_1, *etc.* pigment includes chlorophyll, carotenoid, xanthophyll, *etc.* aromatic includes but not limited to alcohol, aldehydes, acids, and ketone.

Table S2. Comparison of the content of important chemical components.

Green tea [a]	TPs (%)	AA (%)	Ca^{2+} (μg/mL) [b]	$H_2PO_4^-$	Protein
WT	~18.1	~7.4	~7.5	-	-
LJ	~17.0	~6.5	~8.0	-	~1.2%
GGN	-	-	-	-	-
BLC	-	-	~8.3	-	-

[a] Anji white tea (WT), longjing tea (LJ), gougunao tea (GGN), and biluochun tea (BLC) are known as four typical kinds of green tea. [b] Ca^{2+}, one of the minerals, is the main metal ion that participates in the formation of tea cream and sediment on cooling or concentration.[25]

7. The EDX spectra of the GTSN

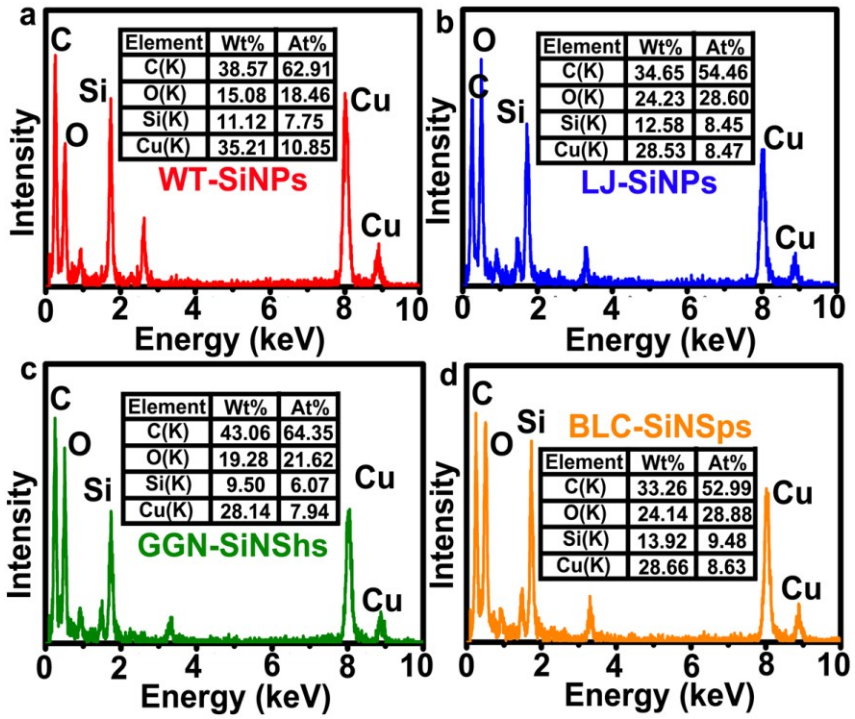

Figure S5. The EDX spectra of the as-prepared GTSN. A typical EDX pattern of the prepared WT-SiNPs (a), LJ-SiNPs (b), GGN-SiNShs (c), and BLC-SiNSps (d). Inset table presents the corresponding elemental ratios (weight and atom percentage) calculated by the EDX software (K-shell intensity ratios are indicated). The EDX pattern qualitatively demonstrates the existence of Si and O in the WT-SiNPs (a), LJ-SiNPs (b), GGN-SiNShs (c), and BLC-SiNSps (d). Nevertheless, it is worthwhile to point out that, for EDX measurement, a quantitative analysis of the elemental ratios is not possible since the supporting substrate (e.g., carbon-coated copper girds) was carbon containing a measurable amount of residual oxygen. Therefore, the element weight concentrations listed in the table are not reliable.

The EDX pattern reveals that four kinds of GTSN all contain Si and O element of ~9.50-13.92% and ~15.08-24.14 % wt concentration, respectively (Figure S5). The C and Cu weight concentrations listed in the table are not reliable since carbon-coated copper grids are used for the EDX measurement.

8. The XPS spectra of the GTSN

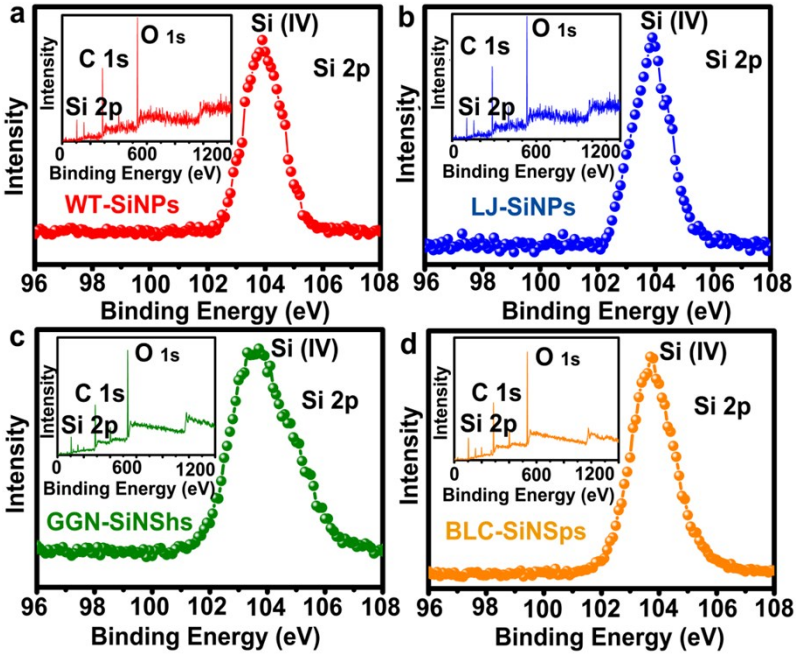

Figure S6. The XPS spectra of the fluorescent GTSN. XPS spectra of WT-SiNPs (a), LJ-SiNPs (b), GGN-SiNShs (c), and BLC-SiNSps (d).

The XPS spectra (Figure S6) of four types of GTSN samples show one peak at ~104 eV, which is defined to oxides of silicon and implies silica composition of the prepared GTSN.

9. The FTIR spectra of the GTSN

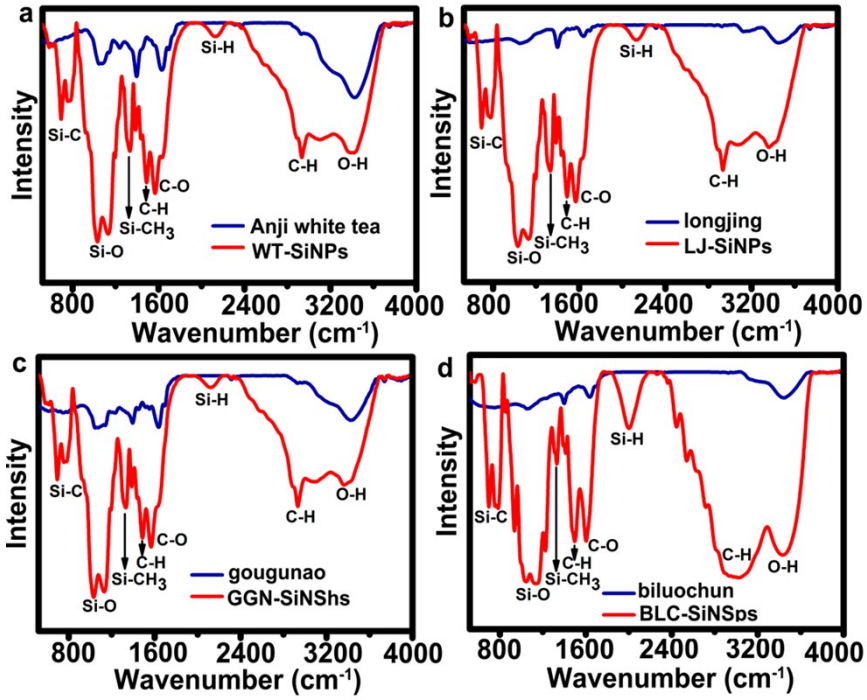

Figure S7. The FTIR spectra of the fluorescent GTSN. FTIR spectra of WT-SiNPs (a), LJ-SiNPs (b), GGN-SiNShs (c), and BLC-SiNSps (d).

As depicted in Figure S7, several identical absorption peaks in the range of 1000-3500 cm^{-1} are observed in WT-SiNPs, LJ-SiNPs, GGN-SiNShs, and BLC-SiNSps, including Si-O vibrations at 1000-1200 cm^{-1}, C-O bands at 1390-1540 cm^{-1} and O-H bands at 3000 cm^{-1}. Compared with FITR spectra of pure Anji white tea drinks, pure longjing tea drinks, pure gougunao tea drinks and pure biluochun tea drinks, there are not more identical absorption peaks (Figure S7).

10. Concentration determination of the GTSN

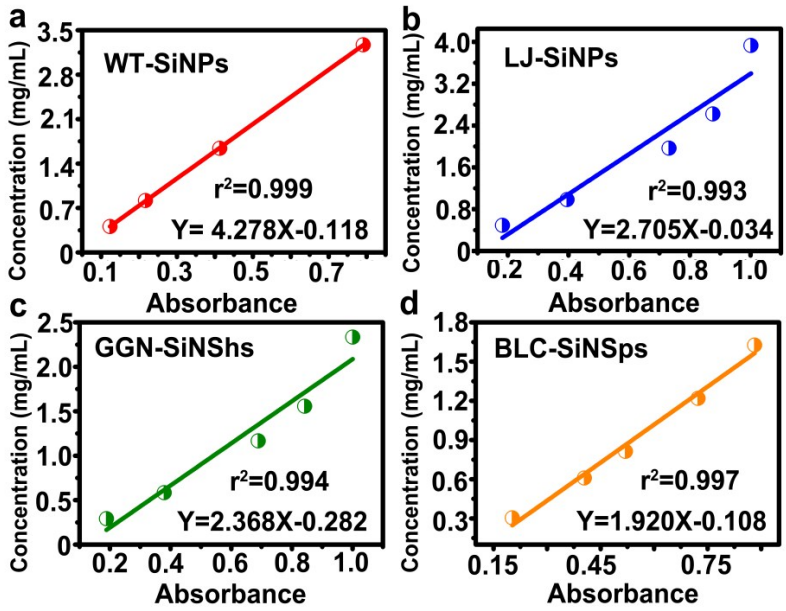

Figure S8. Concentration determination of the fluorescent GTSN. The UV-vis absorbance spectra of WT-SiNPs, LJ-SiNPs, GGN-SiNShs, and BLC-SiNSps versus different concentrations. Concentration vs. absorbance of WT-SiNPs (a), LJ-SiNPs (b), GGN-SiNShs (c), and BLC-SiNSps (d). Solid line is the linear fit using the analysis tool in Origin software.

As shown in Figure S8, WT-SiNPs, LJ-SiNPs, GGN-SiNShs, and BLC-SiNSps with different concentrations are quantified by UV-vis absorbance, which can be used for determining accurate concentrations of the as-prepared samples (Figure S8). [1,2] Figure S8 presents four different linear equation related to concentrations and UV-vis absorbance. Taken WT-SiNPs as an example, corresponding linear equation is about Y = 4.278X - 0.118 mg/mL (Y represents concentrations, X represents UV-vis absorbance) and the corresponding coefficients r^2 = 0.999 (Figure S8a). Other three types of GTSN have the similar linear equation, as shown in Figures S8b, 8c, and 8d.

11. Photoluminescent quantum yields (PLQY) measurements

PLQY, well considered as an important factor for quantitatively evaluating fluorescent intensity of materials, equals to the ratio of the number of emitted photons and the number of absorbed photons. In our experiment, a well-established reference method was employed for determining the PLQY value of four kinds of the resultant GTSN (e.g., WT-SiNPs, LJ-SiNPs, GGN-SiNShs, and BLC-SiNSps) as follow (Quinine sulfate in 0.1 M H_2SO_4 (literature quantum yield: 58%)). [1, 2]

$$\Phi_x=\Phi_{st} (I_x / I_{st}) (\eta_x / \eta_{st})^2 (A_{st} / A_x) \quad \text{.....(S1)}$$

Where Φ is the QY, "I" is the integrated emission intensity, "η" is the refractive index of the solvent, and A is the optical density. The subscript "st" and "x" stand for standard with known QY and the four kind of GTSN (e.g., WT-SiNPs, LJ-SiNPs, GGN-SiNShs, and BLC-SiNSps) sample, respectively. To minimize reabsorption effects, absorption value at the excitation wavelength is required to be smaller than 0.10.

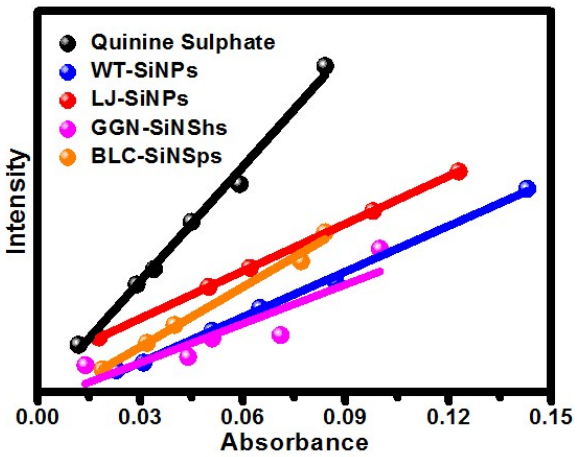

Figure S9. The PLQY measurements of the prepared GTSN. PLQY measurements of WT-SiNPs, LJ-SiNPs, GGN-SiNShs, and BLC-SiNSps. PLQY values of the WT-SiNPs, LJ-SiNPs, GGN-SiNShs, and BLC-SiNSps are calculated by comparing the integrated fluorescence intensities and the absorbance values of WT-SiNPs, LJ-SiNPs, GGN-SiNShs and BLC-SiNSps, respectively. Quinine sulfate in 0.1 M H_2SO_4 (literature quantum yield: 58%) is chosen as the reference and freshly prepared to reduce the measurement error. The solid lines represent the fitting results for each set of data.

As shown in Figure S9, these PLQY values of the WT-SiNPs, LJ-SiNPs, GGN-SiNShs, and BLC-SiNSps are calculated by comparing the integrated fluorescence intensities and the absorbance values of WT-SiNPs, LJ-SiNPs, GGN-SiNShs, and BLC-SiNSps with quantum yield standard, respectively. Notably, the PLQY of WT-SiNPs, LJ-SiNPs, GGN-SiNShs, and BLC-SiNSps are calculated as ~23%, ~24%, ~19%, and ~30%, respectively.

12. Destruction of cellular cytoskeleton

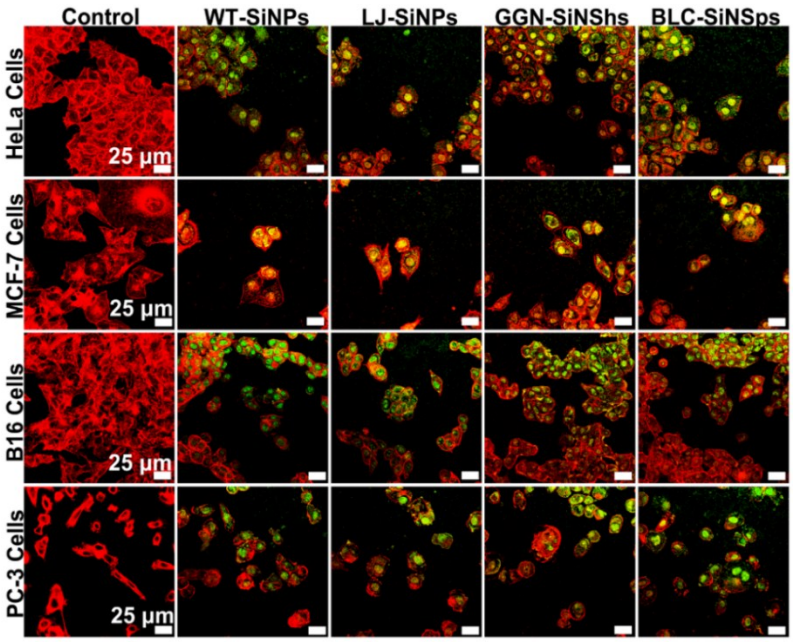

Figure S10. Destruction of cellular cytoskeleton of cancer cells. Confocal images of cellular cytoskeleton of cancer cells (e.g., HeLa, MCF-7, B16, and PC-3 cells). These cancer cells are treated with four kinds of GTSN (e.g., WT-SiNPs, LJ-SiNPs, GGN-SiNShs, and BLC-SiNSps) for 24 h. The cellular nuclei and actin are stained with the fluorescent GTSN (green fluorescent signals) and rhodamine-phalloidin (red fluorescent signals), respectively. Scale bars, 25 μm.

As displayed in Figure S10, for pure medium groups (without any treatment), cancer cells (e.g., HeLa, MCF-7, PC-3, and B16 cells) all show a network of well-formed stress fibers of normal filamentous morphology. In contrast, for GTSN-treated groups, the cellular cytoskeleton of cancer cells appears partially depolymerized with incomplete stress fibers in most cells, indicating their considerable killing ability for cancer cells (e.g., HeLa, MCF-7, B16, and PC-3 cells).

13. Cell cycle distribution of cancer cells treated by the GTSN

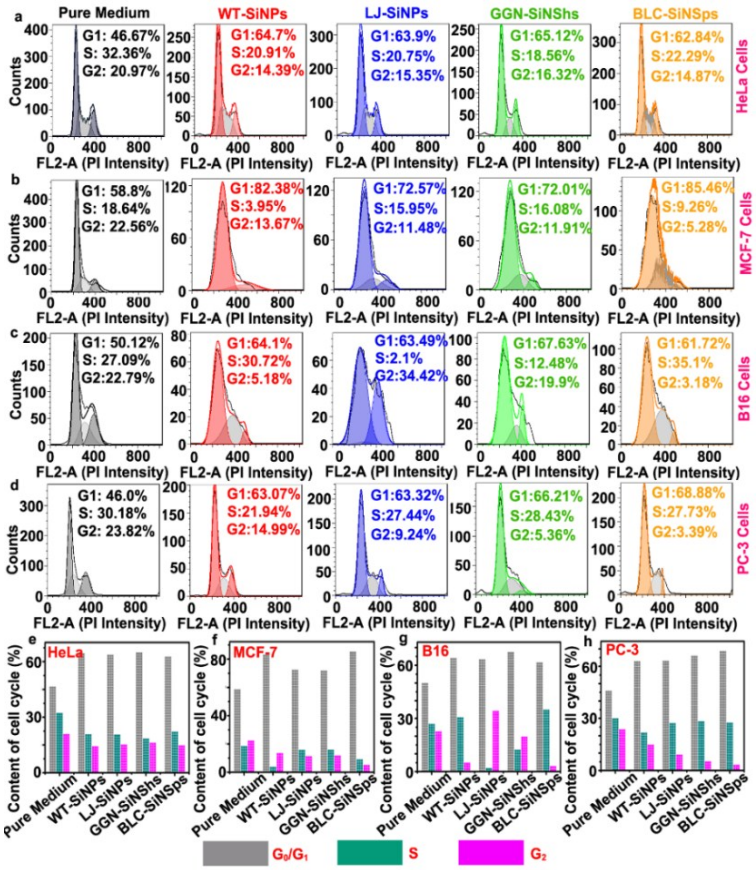

Figure S11. Cell cycle distribution of cancer cells treated by four types of GTSN. Cell cycle distribution of HeLa (a), MCF-7 (b), B16 (c), and PC-3 (d) cells treated with pure medium and four types of GTSN (e.g., WT-SiNPs, LJ-SiNPs, GGN-SiNShs, and BLC-SiNSps) of the concentration at 2.50 mg/mL for 12 h, respectively. Corresponding histograms of cell cycle distribution of HeLa (e), MCF-7 (f), B16 (g), and PC-3 (h) cells originated from Figure S11a-d.

The flow cytometry is further used to examine the effects of four kinds of GTSN on the cell cycle phases (Figure S11). In detail, percentage of G1 phase of cancer cells in pure medium is ~47% (HeLa cells), ~59% (MCF-7 cells), ~50% (B16 cells), or ~46% (PC-3 cells), respectively. After incubated with the fluorescent GTSN, the percentages of G1 phase increase to ~63% (HeLa cells), ~72% (MCF-7 cells), ~62% (B16 cells), and ~63% (PC-3 cells), respectively. These results demonstrate that the cell cycle of cancer cells is arrested at G1 phase when they are treated with four kinds of GTSN for 12 h, suggesting the fluorescent GTSN could inhibit proliferation of cancer cells by arresting the cell cycle at G1 phase.

14. Cytotoxicity of normal cells treated by GTSN

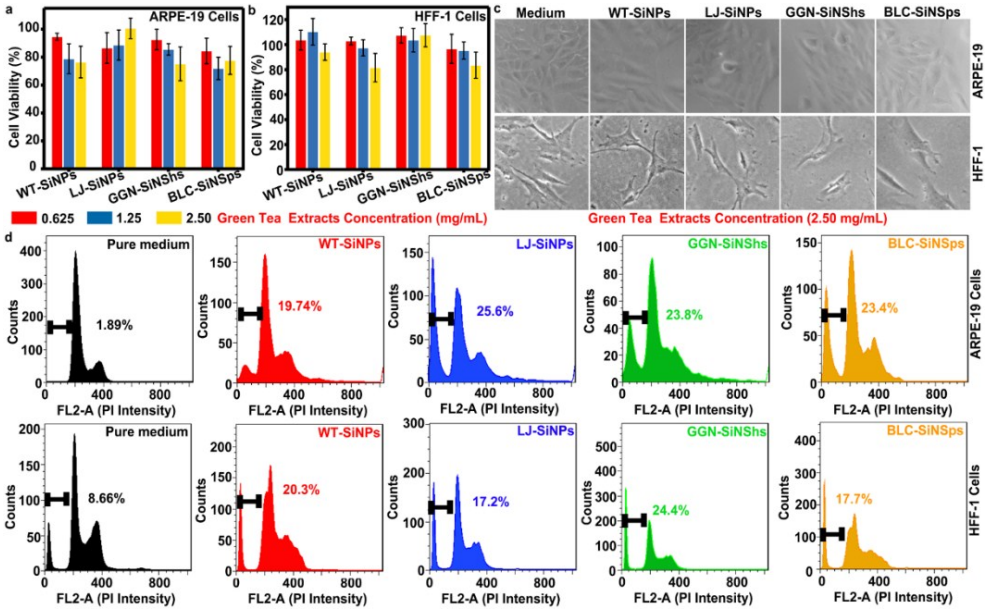

Figure S12. Cytotoxicity of normal cells treated by the resultant GTSN. (a-b) MTT assay results of normal cells (e.g., ARPE-19 and HFF-1 cells) treated with the as-prepared GTSN (e.g., WT-SiNPs, LJ-SiNPs, GGN-SiNShs, and BLC-SiNSps) with various concentrations (e.g., 0.625, 1.25, and 2.50 mg/mL) for 24 h. (c) Cellular morphology of normal cells treated with pure medium and the resultant GTSN (e.g., WT-SiNPs, LJ-SiNPs, GGN-SiNShs, and BLC-SiNSps) at the concentration of 2.50 mg/mL for 24 h. (d) Cell cycle distribution of normal cells treated with pure medium and four types of GTSN at the concentration of 2.50 mg/mL for 24 h, respectively.

We further reveal that the as-prepared GTSN produce feeble toxicity to normal cells. As shown in Figures S12a-b, at the concentration of 2.50 mg/mL, the cellular viability of live normal cells treated by the prepared GTSN (e.g., WT-SiNPs, LJ-SiNPs, GGN-SiNShs, and BLC-SiNSps) is larger than ~80%. Meanwhile, GTSN-treated normal cells preserve integrated morphology, like those of pure medium-treated groups (Figure S12c). Furthermore, as exhibited in Figure S12d, in comparison to slight cell apoptosis and death of normal cells (e.g., ~20-26% of ARPE-19 cells and ~17-24% of HFF-1 cells), the fluorescent GTSN can induce more serious cell apoptosis/death of cancer cells (e.g., larger than ~44-60% of HeLa cells, ~77-93% of MCF-7 cells, ~56-62% of B16 cells, and ~48-62% of PC-3 cells). These results suggest significant and specific anti-cancer efficacy of the resultant GTSN, which is due to well-recognized anti-cancer activity of green tea in vitro.

15. MTT assay of pure green tea solutions

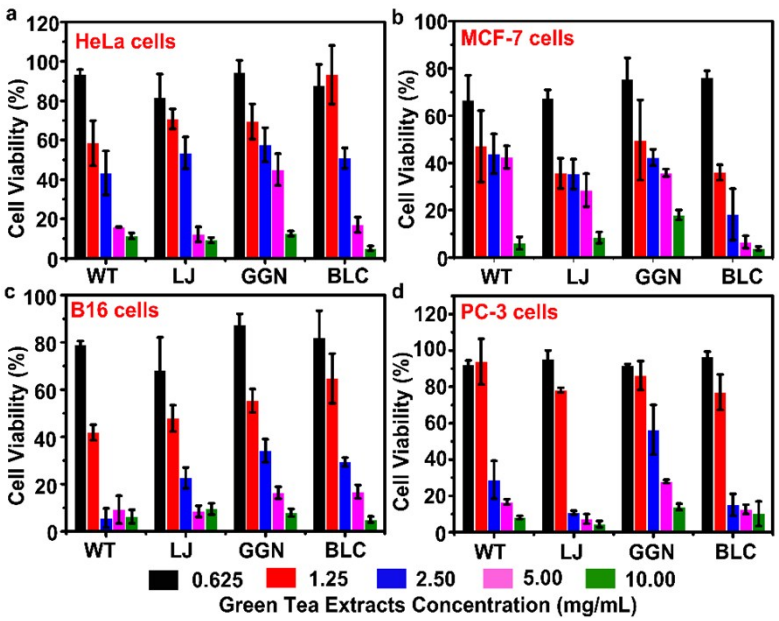

Figure S13. MTT assay of four kinds of pure green tea solutions. The concentration-dependent cell viability of HeLa (a), MCF-7 (b), B16 (c), and PC-3 (d) cells treated with four kinds of pure green tea solutions (e.g., WT, LJ, GGN, and BLC) with various concentrations (e.g., 0.625, 1.25, 2.50, 5.00, and 10.00 mg/mL) for 24 h. All error bars represent the standard deviation determined from three independent assays.

As shown in Figure S13, at the concentration of 10.00 mg/mL, the percentage of live cancer cells (e.g., HeLa, MCF-7, B16, and PC-3 cells) treated with pure WT, LJ, GGN, and BLC solutions is lower than ~20%, respectively. Thus, these results reveal that pure green tea solutions feature concentration-dependent cytotoxicity for cancer cells (e.g., HeLa, MCF-7, B16, and PC-3 cells).

16. Cell growth assay of pure green tea solutions

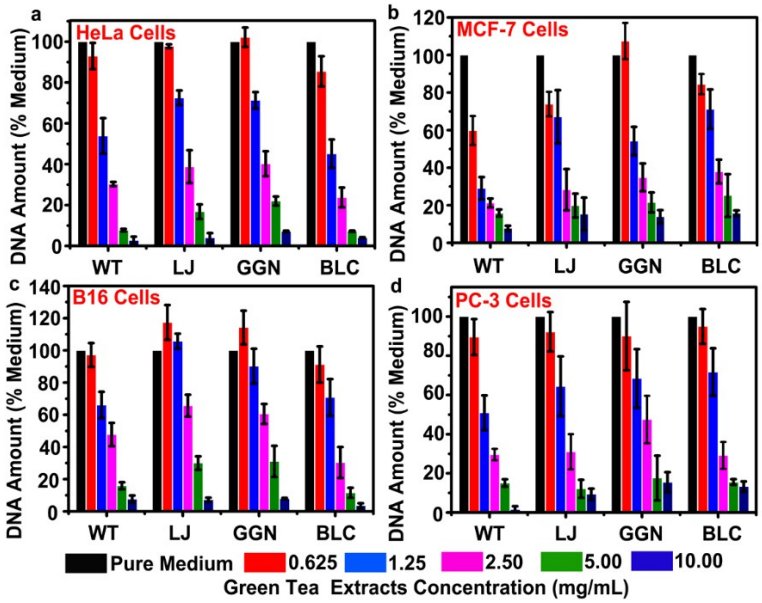

Figure S14. Cell growth assay of four kinds of pure green tea solutions. The concentration-dependent cell viability of HeLa (a), MCF-7 (b), B16 (c), and PC-3 (d) cells treated with four kinds of pure green tea solutions (e.g., WT, LJ, GGN, and BLC) with various concentrations (e.g., 0.625, 1.25, 2.50, 5.00, and 10.00 mg/mL) for 24 h. All error bars represent the standard deviation determined from three independent assays.

As shown in Figure S14, the DNA amount of cancer cells (e.g., HeLa, MCF-7, B16, and PC-3 cells) treated by pure green tea solutions (e.g., WT, LJ, GGN, and BLC solutions) with various concentrations show distinct decreases, compared to the control groups. These results suggest that pure green tea solutions possess concentration-dependent cytotoxicity for cancer cells (e.g., HeLa, MCF-7, B16, and PC-3 cells).

17. Cellular morphology of cancer cells treated with green teas

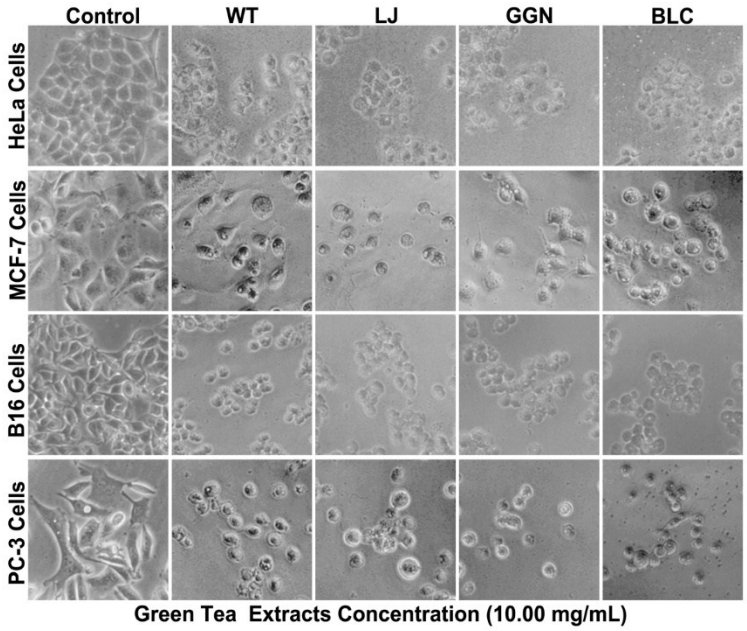

Figure S15. Cellular morphology of cancer cells treated with pure green tea solutions. Morphology of HeLa, MCF-7, B16, and PC-3 cells treated with pure medium and pure green tea solutions (e.g., WT, LJ, GGN, and BLC solutions) at the concentration of 10.00 mg/mL for 24 h.

As presented in Figure S15, the cellular morphologies of cancer cells (e.g., HeLa, MCF-7, B16, and PC-3 cells) without any treatment maintain full and well after 24-h incubation. On the contrary, different cancer cells treated with pure green tea solutions (e.g., WT, LJ, GGN, and BLC solutions) turn into a small sphericity, revealing that pure green tea solution has abilities to kill cancer cells (i.e., HeLa, MCF-7, B16, and PC-3 cells).

18. Cell apoptosis of cancer cells treated with green teas

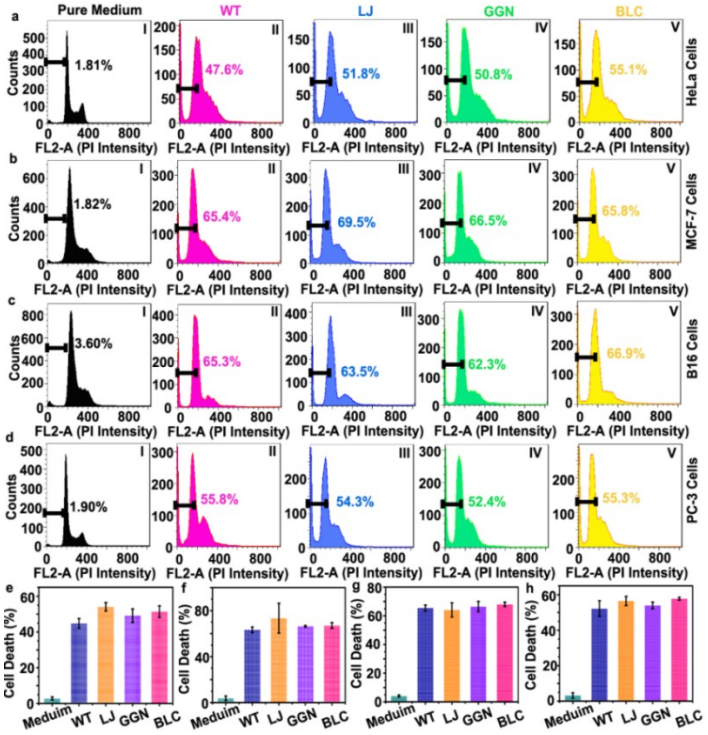

Figure S16. Cell cycle distribution of cancer cells treated with pure green tea solutions. Cell cycle distribution of HeLa (a), MCF-7 (b), B16 (c), and PC-3 (d) cells treated with pure medium and pure green tea solutions (i.e., WT, LJ, GGN, and BLC solutions) of the concentration at 2.50 mg/mL for 24 h, respectively. Corresponding histograms of cell death of HeLa (e), MCF-7 (f), B16 (g), and PC-3 (h) cells originated from Figures S16a-d. All error bars represent the standard deviation determined from three independent assays.

Cancer cells (i.e., HeLa, MCF-7, B16, and PC-3 cells) are firstly treated with pure green tea solutions, and then cell cycle analysis is carried out by propidium iodide (PI) staining and flow cytometry measurement. The cancer cell killing ability of four types of pure green tea solutions (e.g., WT, LJ, GGN, and BLC solutions) is shown in Figure S16. In detail, the pure green tea solutions have abilities to cause ~47.6% (WT), ~51.8% (LJ), ~50.8% (GGN), or ~55.1% (BLC) cell apoptosis and death of HeLa cells (Figure S16a). For MCF-7 cells, significant induction of cell apoptosis and death (e.g., ~65.4% (WT), ~69.5% (LJ), ~66.5% (GGN), or ~65.8% (BLC)) is observed (Figure S16b). Similar tendency can be seen for other two cellular lines (e.g., B16 and PC-3 cells), indicating the pure green tea solutions can also induce cell apoptosis and death (more than ~45%) of cancer cells, which is in contrast to low percentage (~1.81-3.60%) of cell apoptosis/death for pure medium-treated cells (Figures S16a-h).

19. Cell cycle distribution of cancer cells treated with green teas

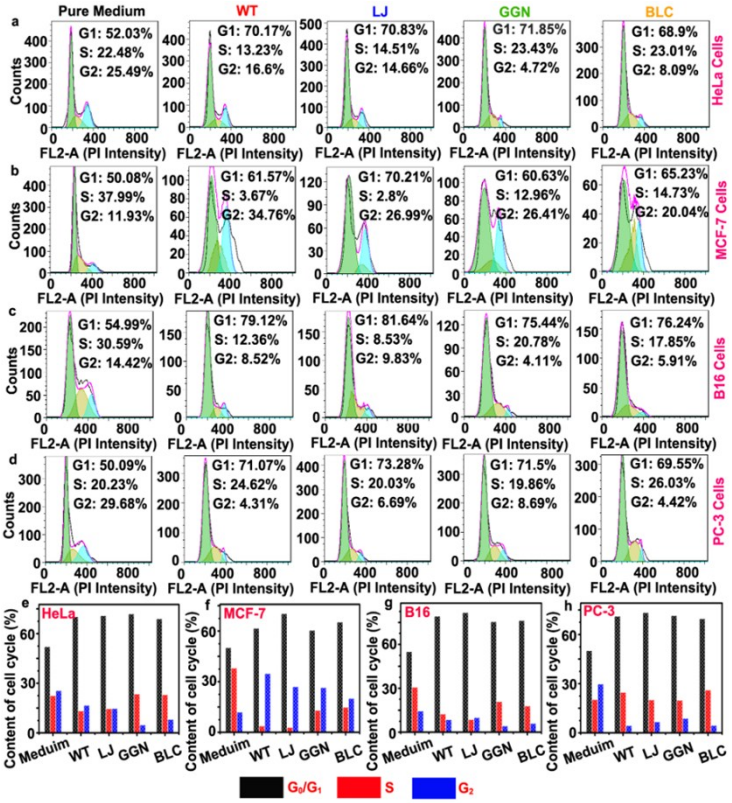

Figure S17. Cell cycle distribution of cancer cells treated with pure green tea solutions. Cell cycle distribution of HeLa (a), MCF-7 (b), B16 (c), and PC-3 (d) cells treated with pure medium and four types of pure green tea solutions (i.e., WT, LJ, GGN, and BLC solutions) of the concentration at 2.50 mg/mL for 12 h, respectively. Corresponding histograms of cell cycle distribution of HeLa (e), MCF-7 (f), B16 (g), and PC-3 (h) cells originated from Figure S17a-d. All error bars represent the standard deviation determined from three independent assays.

To clarify the mechanism of pure green tea-related anti-cancer activity, the flow cytometry is further used to examine the precise effect of four kinds of pure green tea solutions on the cell cycle distribution (Figure S17). In detail, percentage of G1 phase of cancer cells in pure medium is ~52.03% (HeLa cells), ~50.08% (MCF-7 cells), ~54.99% (B16 cells), or ~50.09% (PC-3 cells), respectively. After incubated with pure green tea solutions, the percentages of G1 phase increase to ~68.9-71.9% (HeLa cells), ~60.6-70.2% (MCF-7 cells), ~75.4-81.6% (B16 cells), and ~69.6-73.3% (PC-3 cells), respectively. As thus, the cell cycle phases of cancer cells can be arrested at G1 phase when they are treated with four kinds of the pure green tea solutions for 12 h. These results demonstrate that the pure green tea solutions can inhibit proliferation of cancer cells by arresting the cell cycle at G1 phase.

20. Cytotoxicity of normal cells treated by pure green tea solutions

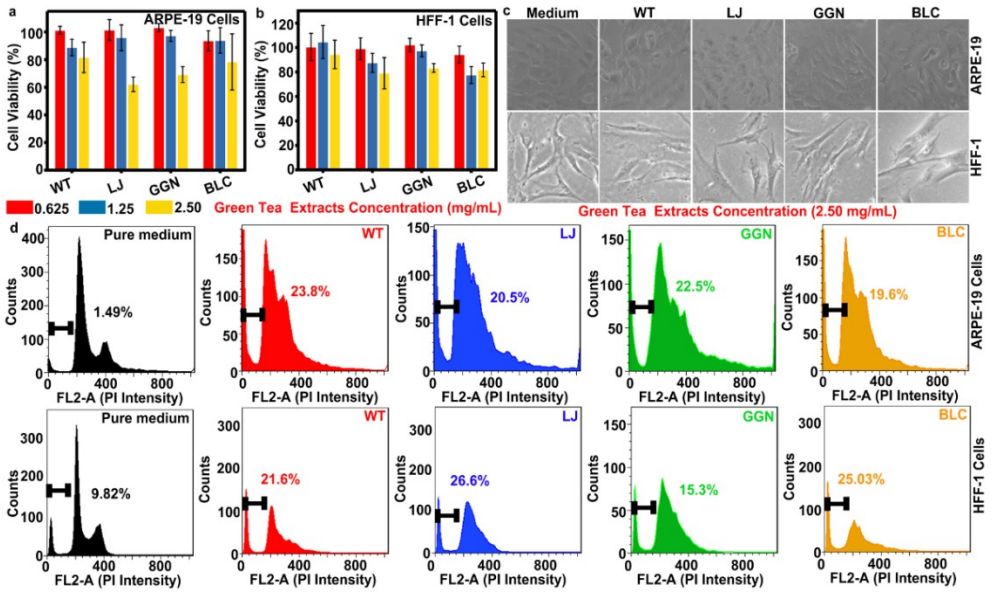

Figure S18. Cytotoxicity of normal cells treated by pure green tea solutions. (a-b) MTT assay results of ARPE-19 and HFF-1 cells treated with pure green tea solutions (e.g., WT, LJ, GGN, and BLC solutions) with various concentrations (e.g., 0.625, 1.25, and 2.50 mg/mL) for 24 h. (c) Morphology of ARPE-19 and HFF-1 cells treated with pure medium and pure green tea solutions (e.g., WT, LJ, GGN, and BLC solutions) at the concentration of 2.50 mg/mL for 24 h. (d) Cell cycle distribution of ARPE-19 and HFF-1 cells treated with pure medium and pure green tea solutions at the concentration of 2.50 mg/mL for 24 h, respectively.

We further reveal that pure green tea solutions (e.g., WT, LJ, GGN, and BLC solutions) produce feeble toxicity to normal cells. As shown in Figures S18a-b, at the concentration of 2.50 mg/mL, the cellular viability of live normal cells treated by pure green tea solutions is larger than ~65-95%. Meanwhile, pure green tea solutions-treated normal cells preserve integrated morphology, like that of pure medium-treated groups (Figure S18c). Furthermore, Figure S18d exhibit that pure green tea solutions only have induced negligible cell apoptosis and death of cancer cells (e.g., ~19-23% of ARPE-19 cells and ~15-26% of HFF-1 cells). These results demonstrate that four kinds of green tea solutions possess negligible cytotoxicity to normal cells (e.g., ARPE-19 and HFF-1 cells).

21. Cell imaging of the fluorescent BLC-SiNSps

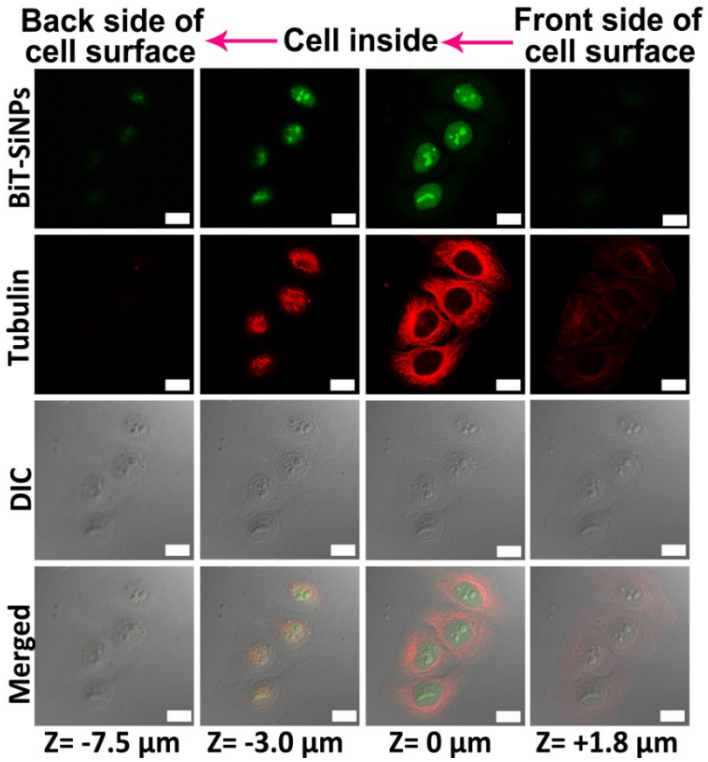

Figure S19. Cell imaging of the fluorescent BLC-SiNSps. Confocal pictures of cellular nuclei imaging and 3D reconstitution of BLC-SiNSps. Scale bars, 7.5 µm.

As presented in Figure S19, weak fluorescence can be detected on the front side of cell surface (Z-axis of +1.8 µm). As the scan proceeds towards the inner layer of HeLa cells, the green fluorescence gradually increases. When the Z-axis changes to 0 µm, the strongest green fluorescence can be imagined in HeLa cells. After that, the green fluorescence becomes weaker as the scan proceeds to the back side of cell surface (Z-axis of -7.5 µm). These results reveal that the as-prepared BLC-SiNSps can directly enter cell nuclei and finally locate in cell nuclei, rather than simply adsorbing to the cell surface.

22. Cellular uptake of the fluorescent GTSN

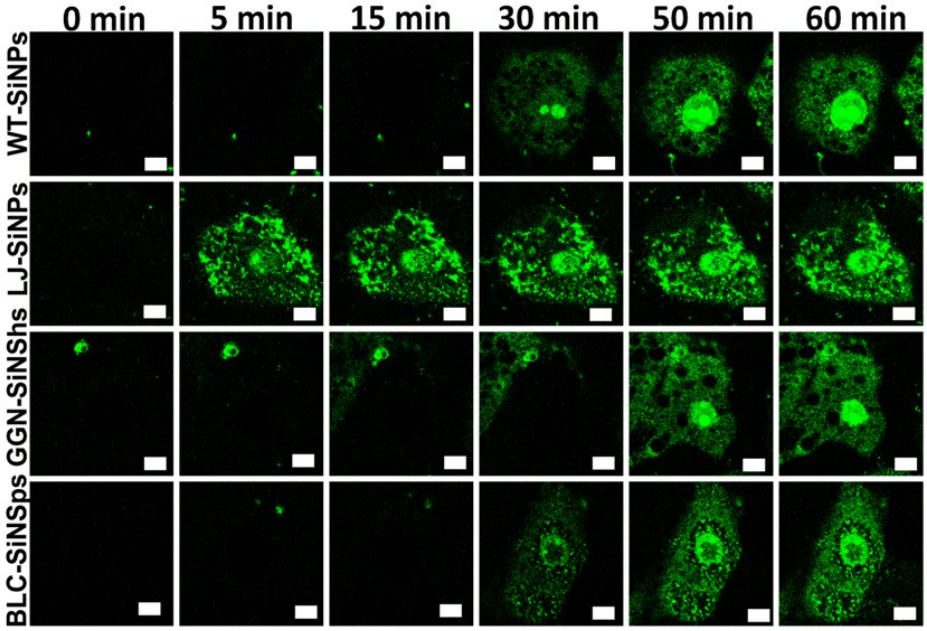

Figure S20. Cellular uptake of the fluorescent GTSN. Long-term and real-time cellular uptake of four types of the prepared GTSN (e.g., WT-SiNPs, LJ-SiNPs, GGN-SiNShs and BLC-SiNSps) in HeLa cells for 60 min. The concentration is 10.00 mg/mL. The time interval is 30 sec. The green fluorescence showed in HeLa cells belongs to the resultant GTSN. Scale bars, 7.5 μm.

Based on direct visual co-localization images presented in Figure S20, green fluorescence of GTSN is observed within both nuclei and cytoplasm, respectively. Typically, in the initial 5 min, the fluorescence intensity is only enhanced in the process of LJ-SiNPs-treated cells. As thus, during this period, only the LJ-SiNPs begin entering HeLa cells. Comparatively, longer incubation time (~30 min) leads to gradual internalization in cells of the WT-SiNPs and BLC-SiNSps (Figure S20). Compared with above three GTSN, green fluorescence signal starts to appear in GGN-SiNShs-treated HeLa cells at least ~50 min. Interestingly, green fluorescence signals of different GTSN appear in both nuclei and cytoplasm during the whole cellular uptake process.

23. Cellular uptake of control groups

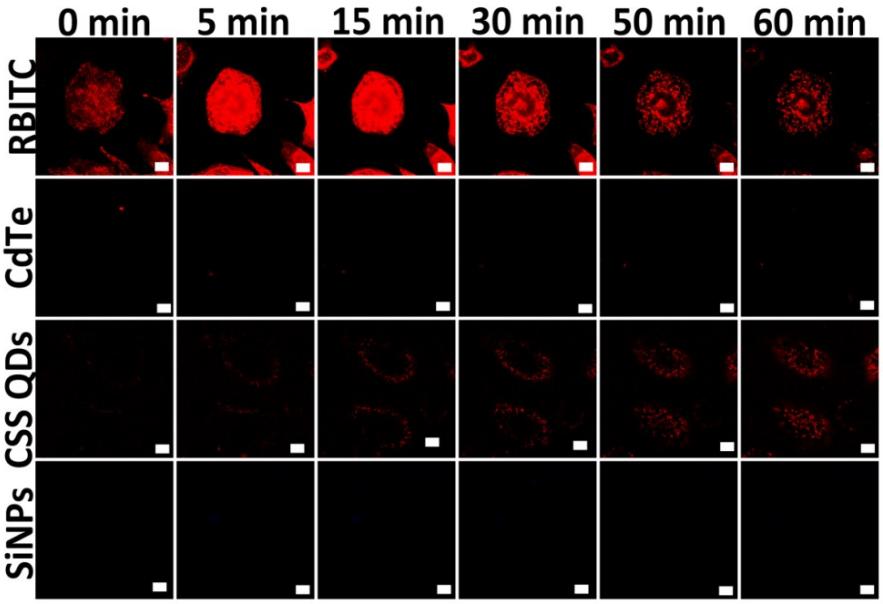

Figure S21. Cellular uptake of control groups. Confocal pictures of cellular uptake of four control groups (e.g., RBITC, CdTe QDs, CSS QDs, and SiNPs) in HeLa cells for 1 h. Scale bars, 10 μm.

Traditional organic dyes (such as RBITC), II-VI quantum dots (such as CdTe QDs and CSS QDs) and the blue-emitting SiNPs prepared through previously reported methods are selected as controls to study cellular uptake pathway. As shown in Figure S21, RBITC enter HeLa cells rapidly in a few minutes. With the time increases, the red fluorescence gradually becomes increasingly stronger. At 15 min, RBITC enter cells totally, exhibiting the strongest red fluorescence. Afterwards, the fluorescent intensity is gradually reduced when time further prolongs. For CSS QDs, red fluorescence becomes gradually stronger in cytoplasm. In contrast, CdTe QDs and SiNPs don't enter cells quickly within 1 h. These results reveal that the resultant GTSN (i.e., WT-SiNPs, LJ-SiNPs, GGN-SiNShs, and BLC-SiNSps) have different cellular uptake pathway from the control groups (i.e., RBITC, CdTe QDs, CSS QDs, and SiNPs).

24. Intracellular distribution of control groups

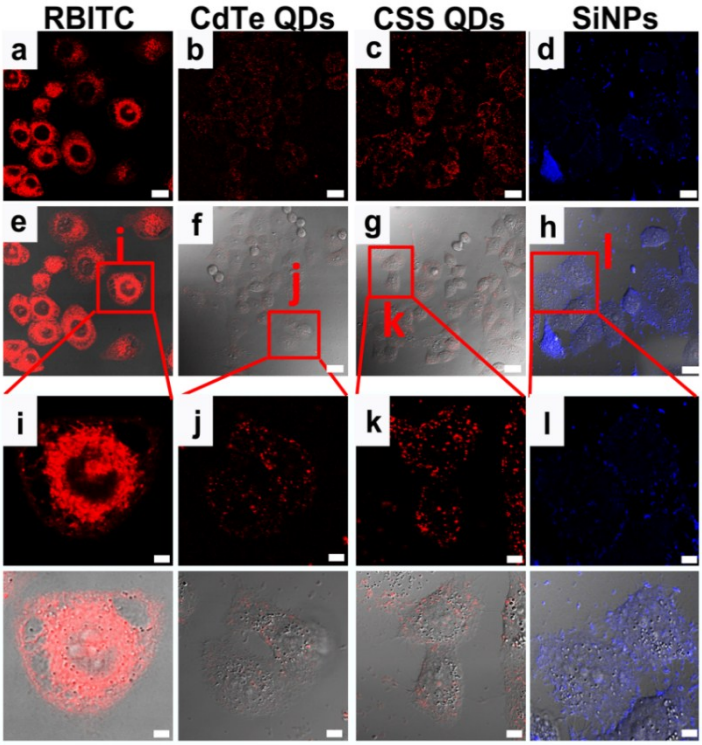

Figure S22. Intracellular distribution of control groups. Confocal pictures of intracellular distribution of four control groups (RBITC, CdTe QDs, CSS QDs, and SiNPs) in HeLa for 5 h. Scale bars, 25 μm (up) and Scale bars, 10 μm (down).

As presented in Figure S22, obvious red fluorescence signals can be observed in cytoplasm and nuclei in RBITC-treated HeLa cells. Different from traditional RBITC dyes, strong red fluorescence of CdTe QDs and CSS QDs can be observed in cytoplasm (Figure S22), indicating that CdTe QDs and CSS QDs mostly locate in cytoplasm of HeLa cells. In comparison, when HeLa cells are incubated with SiNPs, there is negligible blue fluorescence signals appearing in cytoplasm and nuclei, and merely slight blue fluorescence signals are observed in cell membrane.

25. Intracellular distribution of four kinds of GTSN

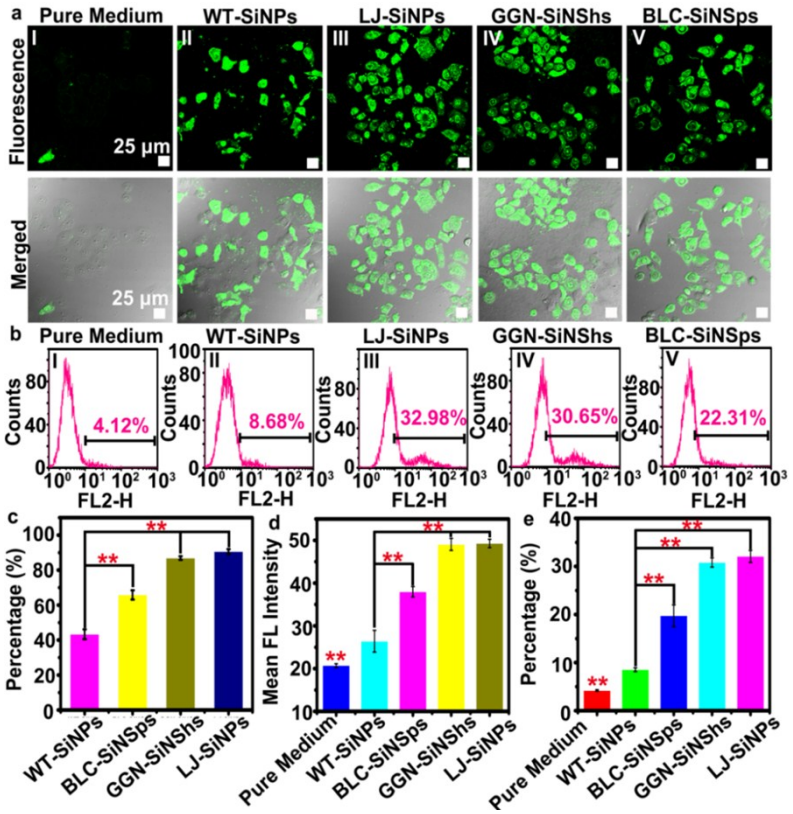

Figure S23. Intracellular distribution of four kinds of GTSN. (a) Confocal pictures of intracellular distribution of the as-prepared GTSN in HeLa cells for 5 h. The concentration is 10.00 mg/mL. The pure medium group means that HeLa cells are cultured in pure medium. Scale bars, 25 μm. (b) Corresponding histograms of HeLa cells treated with pure medium (I), WT-SiNPs (II), LJ-SiNPs (III), GGN-SiNShs (IV), and BLC-SiNSps (V) of the concentration at 10.00 mg/mL obtained via flow cytometry. (c) Corresponding histograms of the percentage for entering nuclei in HeLa cells treated with different GTSN based on counting from Figure 23a. (d) Corresponding histograms of mean fluorescence intensity in HeLa cells treated with pure medium and different GTSN obtained by quantifying Figure S23b. (e) Corresponding histograms of the percentage for entering nuclei in HeLa cells treated with pure medium and different GTSN obtained by quantifying Figure S23b. ** means $p < 0.01$. The error bars show the standard deviation determined from three independent measurements.

26. In vivo imaging of GTSN and pure green tea solutions

Figure S24. In vivo imaging of four types of GTSN and pure green tea solutions. Spectrally unmixed in vivo fluorescence images of 4T1-bearing nude Balb/c mice at different times (i.e., 0, 7, and 14 days) after intratumorally injection of physiological saline (untreated), four kinds of pure green tea solutions (e.g., WT, LJ, GGN, and BLC solutions) and the resultant GTSN (e.g., WT-SiNPs, LJ-SiNPs, GGN-SiNShs, and BLC-SiNSps) at the same dose (i.e., 50 mg/kg).

In our experiment, a single dose (i.e., 50 mg/kg) of physiological saline (untreated), pure green tea solutions (e.g., WT, LJ, GGN, and BLC), and the fluorescent GTSN (e.g., WT-SiNPs, LJ-SiNPs, GGN-SiNShs, and BLC-SiNSps) is intratumorally injected into the tumor issue, respectively. As exhibited in Figure S24, the corresponding intratumorally fluorescence distribution is captured by a Maestro EX in vivo fluorescence imaging system (excited wavelength: 440 and captured wavelength: 450-580 nm). In detail, in comparison to physiological saline (untreated)- and pure green tea solutions-treated group showing no fluorescence, WT-SiNPs, LJ-SiNPs, GGN-SiNShs, and BLC-SiNSps-treated tumor issues exhibit strong fluorescent signals. Importantly, there distinct fluorescent signals are also observed in the fluorescent GTSN-treated tumor issues after during 14-d post injection (Figure S24), demonstrating that the GTSN (e.g., WT-SiNPs, LJ-SiNPs, GGN-SiNShs, and BLC-SiNSps) can accumulate in tumor issues of mice during long-term manners (e.g., 14-d treatment).

27. H & E stained photos of major organs treated with GTSN

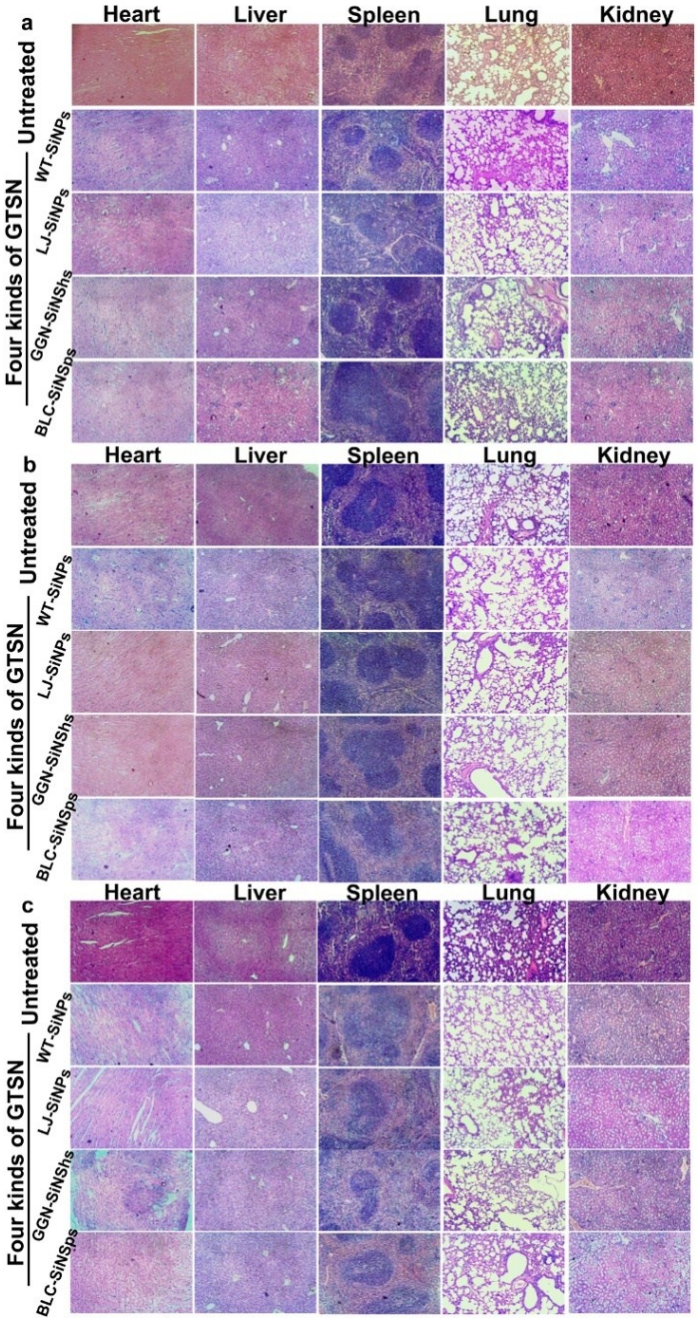

Figure S25. H & E stained photos of major organs harvested from the mice treated with physiological saline (untreated) and four kinds of GTSN. Histological analysis of major organs (e.g., heart, liver, spleen, lung, and kidney) after treatments with physiological saline (untreated) and four kinds of GTSN for 1 (a),7 (b), and 30 (c) days.

28. Serum biochemistry analysis from mice treated with GTSN

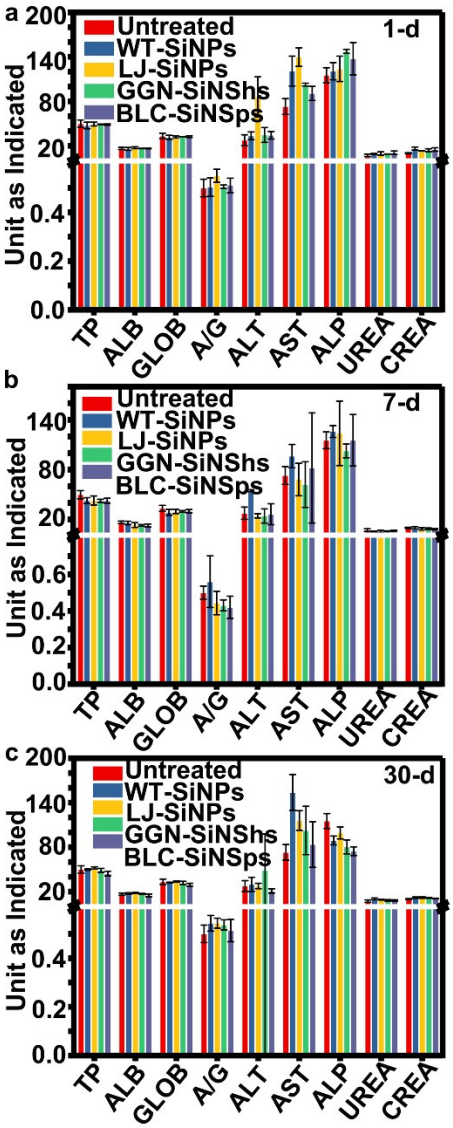

Figure S26. Serum biochemistry analysis from mice treated with physiological saline and four kinds of GTSN. The data show the mean and standard deviation of TP, ALB, GLOB, A/G, ALT, AST, ALP, urea, and crea when the mice are exposed to four types of GTSN (e.g., WT-SiNPs, LJ-SiNPs, GGN-SiNShs, and BLC-SiNSps) or physiological saline (untreated) for 1 (a), 7 (b), and 30 (c) days through intratumorally injection.

29. Hemolysis results of GTSN

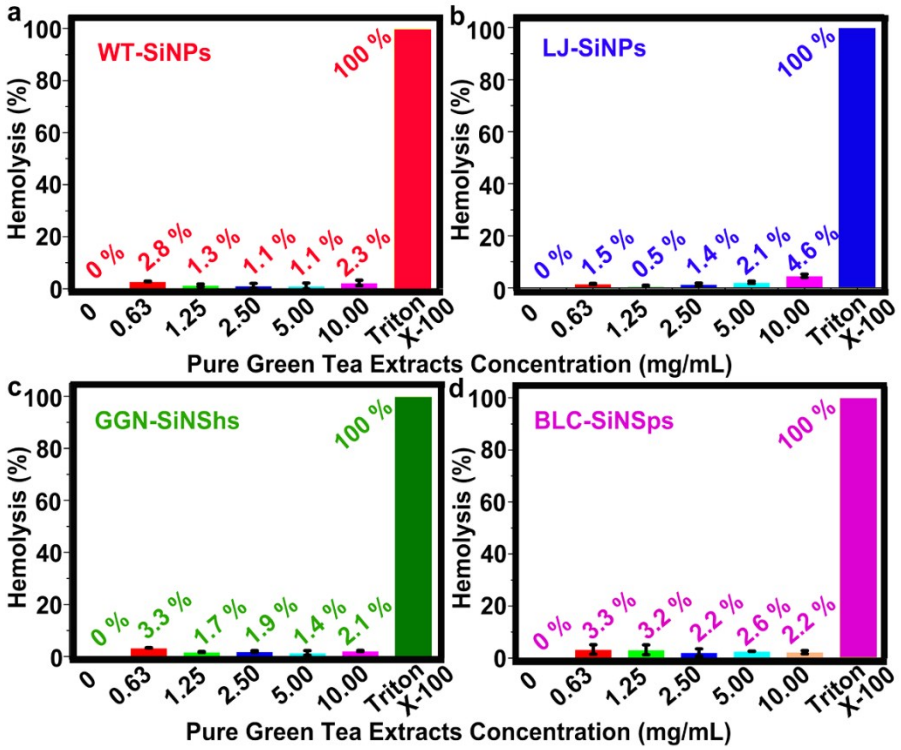

Figure S27. Hemolysis results of these four kinds of GTSN. Hemolysis results of WT-SiNPs (a), LJ-SiNPs (b), GGN-SiNShs (c), and BLC-SiNSps (d) with different concentrations (e.g., 0, 0.63, 1.25, 2.50, 5.00, and 10.00 mg/mL) for 5-h incubation. Normal saline (0.9% NaCl) was set as the negative control. Triton X-100 was set as the positive control. All error bars represent the standard deviation determined from three independent assays.

As suggested in Figure S27, no hemolytic activity is observed for four types of the fluorescent GTSN at various concentrations (e.g., 0, 0.63, 1.25, 2.50, 5.00, and 10.00 mg/mL), revealing that the resultant GTSN have abilities to be further applied in in vivo imaging and cancer therapy.

30. H & E stained photos of major organs treated with green teas

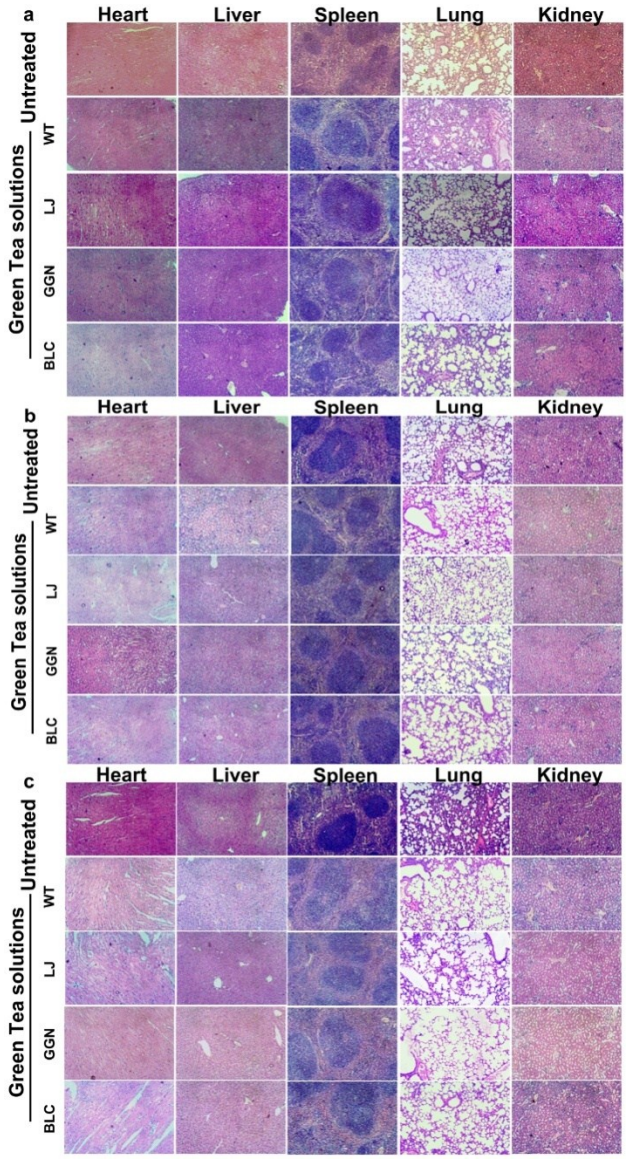

Figure S28. H & E stained photos of major organs harvested from the mice treated with physiological saline (untreated) and four kinds of pure green tea solutions. Histological analysis of major organs (e.g., heart, liver, spleen, lung, and kidney) after treatments with physiological saline (untreated) and four kinds of pure green tea solutions for 1 (a), 7 (b), and 30 (c) days.

31. Serum biochemistry analysis from mice treated with green teas

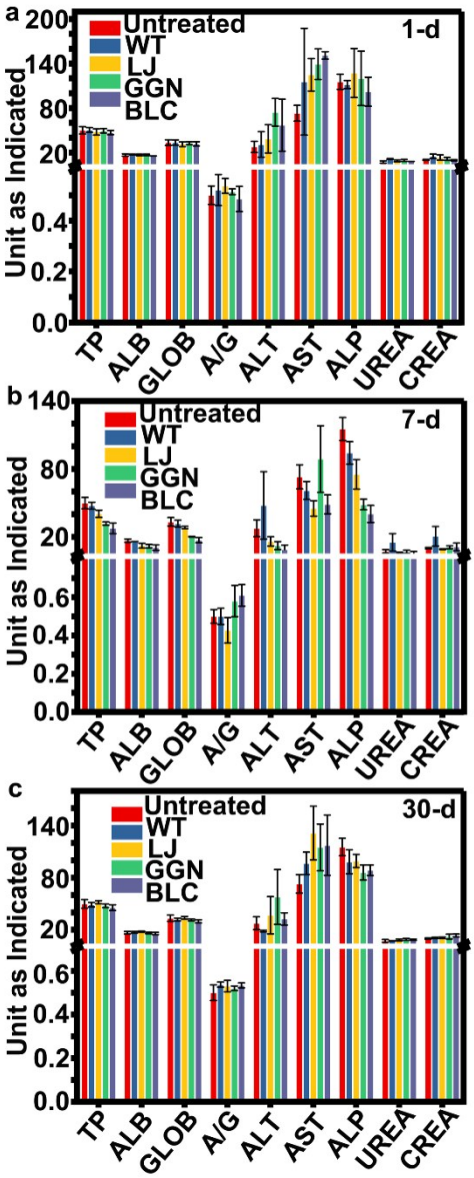

Figure S29. Serum biochemistry analysis from mice treated with physiological saline and four kinds of pure green tea solutions. The data show the mean and standard deviation of TP, ALB, GLOB, A/G, ALT, AST, ALP, urea, and crea when the mice are exposed to four types of pure green tea solutions or physiological saline (untreated) for 1 (a), 7 (b), and 30 (c) days through intratumorally injection.

32. Reference

1 Y. Zhong, F. Peng, F. Bao, S. Wang, X. Ji, L. Yang, Y. Su, S. T. Lee, and Y. He, *J. Am. Chem. Soc.*, 2013, **135**, 8350-8356.

2 Y. Zhong, X. Sun, S. Wang, F. Peng, F. Bao, Y. Su, Y. Li, S. T. Lee and Y. He, *ACS Nano*, 2015, **9**, 5958-5967.

3 S. Wu, Y. Zhong, Y. Zhou, B. Song, B. Chu, X. Ji, Y. Wu, Y. Su and Y. He, *J. Am. Chem. Soc.*, 2015, **137**, 14726-14732.

4 Y. Wu, Y. Zhong, B. Chu, B. Sun, B. Song, S. Wu, Y. Su and Y. He, *Chem. Commun.*, 2016, **52**, 7047-7050.

5 B. Song, Y. Zhong, S. Wu, B. Chu, Y. Su and Y. He, *J. Am. Chem. Soc.,* 2016, **138**, 4824-4831.

6 X. Ji, D. Guo, B. Song, S. Wu, B. Chu, Y. Su and Y. He, *Nano Res.*, 2018, **11**, 5629–5641.

7 M. M. Tomczak, D. D. Glawe, L. F. Drummy, C. G. Lawrence, M. O. Stone, C. C. Perry, D. J. Pochan, T. J. Deming and R. R. Naik, *J. Am. Chem. Soc.,* 2005, **127**, 12577-12582.

8 F. C. Meldrum and H. Cölfen, *Chem. Rev.*, 2008, **108**, 4332-4432.

9 M. B. Dickerson, K. H. Sandhage and R. R. Naik, *Chem. Rev.*, 2008, **108**, 4935-4978.

10 C. Mao, F. Wang and B. Cao, *Angew. Chem. Int. Ed.*, 2012, **51**, 6411-6415.

11 B. Liu, Y. Cao, Z. Huang, Y. Duan and S. Che, *Adv. Mater.*, 2015, **27**, 479-497.

12 B. Ghosh, Y. Masuda, Y. Wakayama, Y. Imanaka, J. Inoue, K. Hashi, K. Deguchi, H. Yamada, Y. Sakka, S. Ohki, T. Shimizu and N. Shirahata, *Adv. Funct. Mater.*, 2014, **24**, 7151-7160.

13 X. H. Yang, Q. S. Wu, L. Li, Y. P. Ding and G. X. Zhang, *Colloids and Surfaces A: Physicochem. Eng. Aspects*, 2005, **264**, 172-178.

14 L. Travaglini and L. De Cola, *Chem. Mater.*, 2018, **30**, 4168-4175.

15 G. Zan and Q. Wu, *Adv. Mater.*, 2016, **28**, 2099-2147.

16 H. N. Graham, *Prev. Med.,* 1992, **21**, 334-350.

17 H. Horie, T. Mukai and K. Kohata, *J. Chromatogr. A*, 1997, **758**, 332-335.

18 J. F. Yin, Y. Q. Xu, H. B. Yuan, L. X. Luo and X. Qian, *J. Food Chem.*, 2009, **114**, 665.

19 Y. Zhao, P. Chen, L. Lin, J. M. Harnly, L. Yu and Z. Li, *Food Chem.*, 2011, **126**, 1269-1277.

20 M. S. El-Shahawi, A. Hamza, S. O. Bahaffi, A. A. Al-Sibaai, T. N. Abduljabbar, *Food Chem.*, 2012, **134**, 2268-2275.

21 Y. Q. Xu, W. B. Ji, P. Yu, J. X. Chen, F. Wang and J. F. Yin, *Food Chem.*, 2018, **248**, 146-154.

22 A. Alcázar, O. Ballesteros, J. M. Jurado, F. Pablos, M. J. Martín, J. L. Vilches and A. Navalón, *J. Agric. Food Chem.,* 2007, **55**, 5960-5965.

23 Y. R. Liang, Z. S. Liu, Y. R. Xu and Y. L. Hu, *J. Sci. Food. Agric.*, 1990, **53**, 541-548.

24 L. Yao, X. Liu, Y. Jiang, N. Caffin, B. D'Arcy, R. Singanusong, N. Datta and Y. Xu, *Food Chem.*, 2006, **94**, 115-122.

25 Y. Q. Xu, X. Y. Zhong, J. F. Yin, H. B. Yuan, P. Tang and Q. Z. Du, *Food Chem.,* 2013, **139**, 944-948.